Geosciences Journal
Vol. 20, No. 4, p. 539 − 549, August 2016
DOI 10.1007/s12303-015-0070-x

Numerical analysis on scale effect of elasticity, strength and failure patterns of jointed rock masses

Peitao Wang* — *School of Civil and Environmental Engineering, University of Science and Technology Beijing, Beijing 100083, China; Key Laboratory of High-Efficient Mining and Safety of Metal Mines (Ministry of Education of China), University of Science and Technology Beijing, Beijing 100083, China*

Tianhong Yang, Tao Xu — *School of Resources and Civil Engineering, Northeastern University, Shenyang 110819, China*

Meifeng Cai, Changhong Li — *School of Civil and Environmental Engineering, University of Science and Technology Beijing, Beijing 100083, China; Key Laboratory of High-Efficient Mining and Safety of Metal Mines (Ministry of Education of China), University of Science and Technology Beijing, Beijing 100083, China*

ABSTRACT: It is of great importance to study the failure process and scale effect of jointed rock mass in the field of rock mechanics and mining engineering. In the present paper, initially the uniaxial compression test on granite was performed and acoustic emission (AE) sequence was acquired during the compression process in laboratory. Results from numerical simulations using the particle flow code in two dimensions (PFC2D) were presented, and compared with experimental measurements. It was observed that the approach was reasonably good in predicting the real response of granite rock samples. The mechanical parameter of joint model was then calibrated based on PFC2D model with experimental results. Finally the mechanical properties of complex rocks with discrete fracture network (DFN) were studied and scale effects on the elasticity and strength were then investigated. The result showed that the failure pattern was similar when the ratio of joint contact bond strength (both shear and normal) to rock contact bond strength was in the range of 3~9%. The elastic modulus and strength parameters were changed with the sizes of rock sample for DFN models. Moreover, the variation of rock failure pattern under different sizes was also studied and finally the representative elementary volume (REV) size of the considered rock mass was estimated to be 9 × 9 m. It is suggested that the failure pattern analysis should be considered in the REV study of jointed rock mass.

Key words: jointed rock mass, scale effect, representative elementary volume, failure pattern, particle flow code

1. INTRODUCTION

Rock mass is a geologic body composed of discontinuities which often have profound effects on the elastic and strength properties (Pariseau et al., 2008). Due to the existence of discontinuities, jointed rock mass often exhibits an inherent anisotropy and deformability of rock masses influencing their behavior is an important geomechanical property for the design of rock structures. Geometric and mechanical characterization of rock joints is necessary in dealing with the mechanical properties of jointed rock mass. The lower strength of a rock mass, especially, is caused by the existence and arrangement of rock joints separating the rock mass into parts. In Dershowitz and Einstein's opinion (1988), the ideal characterization of joint would involve the specific description of each joint in the rock mass, exactly defining its geometric and mechanical properties. In foundations of civil structures, underground excavations as well as tunneling, these materials are often unavoidable.

In order to study the influences of occurrence characteristics of discontinuities on deformation and strength of rock mass, extensive numerical methods have been carried out to study rocks (Zhao et al., 2013; Lee and Jeong, 2015) or jointed rock masses (Park and Min, 2012; Xu et al., 2013; Zhang and Wong, 2013; Sarfarazi et al., 2013; Wasantha et al., 2014). Among the numerical methods, the discrete element method has many advantages in modeling rock masses and possessing the ability to fracture and break apart under stress. And it is possible to simulate rock on any scale from intact rock composed of several particles to rock masses. Previous studies with discrete element method have verified that such models are able to describe qualitatively several features observed in physical experiments. For the purpose of a quantitative description, numerical analyses are carried out using PFC2D (particle flow code in two dimensions) version 3.10. PFC2D models the movement and interaction of circular particles by the distinct element method and is a logical choice for modeling the mechanical behavior. The code (Cundall and Strack, 1979) represents a rock mass as an assemblage of circular disks confined by planar walls and models the forces and motions of the particles within this assembly. Particles move independently and could interact at contact with others. Two basic bonding models are adopted in PFC2D, viz. a contact-bond model and a parallel-bond model (Itasca Consulting Group, Inc., 2004). Both bonds can be envisioned as a kind

*Corresponding author: 124828649@qq.com

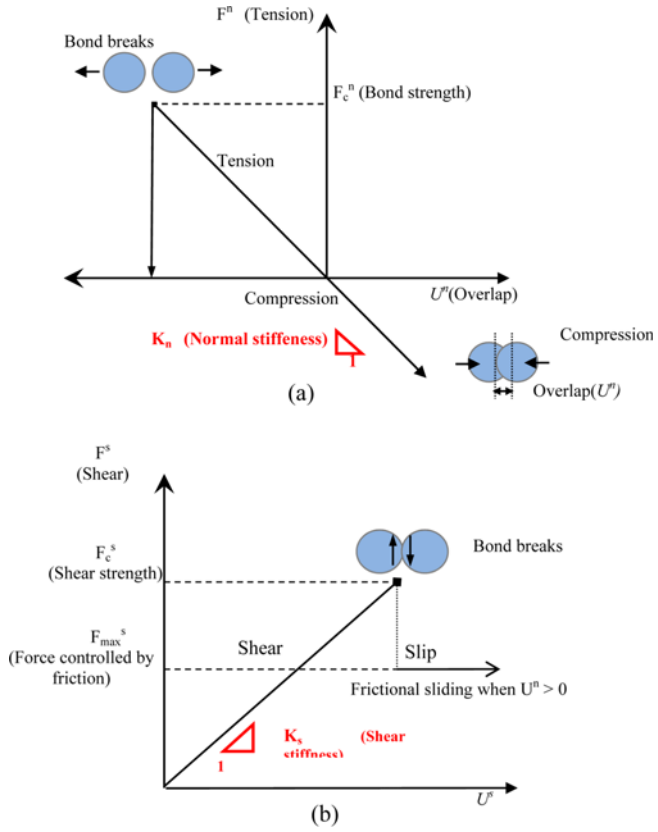

Fig. 1. Constitutive behavior for bonded particle model in PFC2D: (a) Normal component of contact force; (b) Shear component of contact force.

of glue joining two particles. The parallel bond model can effectively characterize the transmission of moments between particles and thus can describe the constitutive of a finite-sized piece of cementitious material such as concrete. However, this model needs more parameters to be calibrated. In the contact bond model, the contact bonds could be envisaged as a pair of elastic springs with constant normal and shear stiffness acting at the contact point. Hazzard et al. (2000) verified the feasibility of using the contact bonded particle models to reproduce mechanical behaviors on different rock types. In the contact bond model, the stiffness could influence the macro mechanical properties such as Young's modulus and Poisson's ratio. Figure 1 shows the constitutive behavior for the contact bond model in PFC2D according to Itasca Consulting Group, Inc. (2004). The contact existing between particles could break when force is over the bond strength. In this way, the deformation and fracture of rock could be simulated. In this study, the contact bond model will be used to study the mechanical behavior of rock mass. PFC method incorporates mesoscopic mechanical parameters different from macro mechanical parameters. Althouth it is relatively easy to assign mesoscopic parameters to a PFC model, nevertheless, it is difficult to choose such properties so that the behavior of the assembles is accordant with that of an intended rock specimen. In this case, we must first determine mechanical properties of the intended rock specimen, and then choose the appropriate mesoscopic paremeters in PFC by means of a calibration process. Such a calibration has to consist of a comparison between numerical and controlled physical experiments, where the numerical model are as much as possible equivalent to the physical model material. If a quantitative match between numerical simulaiton and physical experiments is obtained, there is further potential for obtaining quantitatively correct results also in simulation of more complex materials, like natural rock (Holt et al., 2005). The elastic modulus, corresponding compressive strength (Wang et al., 2003; Holt et al., 2005; Yoon, 2007; Cho et al., 2007; Fakhimi and Gharahbagh, 2011) and the failure patterns (Potyondy and Cundall, 2004; Funatsu and Shimizu, 2012) are usually used as the responses for calibration process. Hazzard and Young (2000) presented a technique for recording the acoustic emisson (AE) during the compressive test using contact bonded particle models on a model of a granite core sample. The particles in this model are bonded together at contact points. When forces exceed the bond strength, the bond breaks. Each bond breakage in PFC2D was considered as a microcrack in the modeled rock. Two types of cracks, viz. shear cracks and tensile cracks, could be obtained in the PFC2D model. The shear crack occurs if a bond's shear strength is exceeded. In the same way, the crack is called a tensile crack when a bond's normal strength is exceeded. All the crack events are considered as AE activities to compare with the experimental results. The feasibility of AE monitoring technique in PFC2D proves that it can also be used in the process of choosing the micro parameters. Notwithstanding, the calibration process is still a time-consuming process and no direct equation is established until the present research.

The objective of this paper is to propose an reasonable approach to assign the scale effects on elasticity and strength of jointed rock mass. Firstly, the laboratory experiments were performed on the rock matrix cored from the rock mass in Heishan open pit mine in Chengde city, China, using the compressive system and AE monitering system. Then, the validated numerical model was used for further study of the mechanical behavior of jointed models with different joints. Failure patterns were used and compared to calibrate the strength parameters of joints. Finally, a case study in the northern slope in Heishan metal mine is taken up. Results from simulations of jointed rock mass using discrete continuum approaches are presented, and the scale effects on elasticity and strength were presented. Moreover, the scale effect on failure patterns was discussed. The results in the present paper will benefit parameter determination in Heishan open pit mine and the further geomechanical study of jointed rock mass.

2. CALIBRATION FOR ROCK MATRIX

It is important to calibrate the numerical model against

the controlled laboratory experiments before systemically studying the mechanical behavior of jointed rock mass. The uniaxial compression experiment was first performed for the calibration for rock matrix obtained from Heishan metal mine. A servo-controlled hydraulic testing machine, namely YAG-3000 with the maximum axial loading of 3000 kN was used in this experiment. Stiffness of the whole machine is more than 30 GN/m and the uniaxial loading rate was 20 kN/min in this work. In parallel with the experiment, the acoustic emission (AE) was monitored during the loading process. AE signals were acquired using PCI-2 system. Eight Nano30 sensors with frequency sensitivity ranging from 125 kHz to 750 kHz and a 40 dB pre-amplification namely 1220A-AST were used in the AE system. Figure 2 shows the schematic diagram of the physical experiments.

The micro-scale properties such as particle size and distribution, particle stiffness, particle friction and bond strengths should be determined to simulate the behavior of rock matrix. A series of numerical tests were performed to simulate the true uniaxial compression. The loading was applied on the numerical specimen through two rigid boundary walls with servo-controlled positions. With the fixed bottom plate, the top plate was moved vertically at a constant deformation rate. Strain and stress variations were computed through wall displacement and resultant forces on walls, respectively. The numerical stress-strain curve compared with the laboratary test is presented in Figure 3a. The uniaxial comressive strength (UCS) is 132.3 MPa and Young's modulus is about 12.0 GPa according to the experimental results. In the simulation, the UCS and Young's modulus is 131.5 MPa and 12.22 GPa, respectively. In addtion, the failure pattern and AE rates compared with the experimental results are alos depicted. The AE events reach a peak rate when the stress is in the range of 105~130 MPa which is observed to be in reasonable accordance with experimental results. According to the results, a good agreement is visualized compared with the measured response of experimental sample and the appropriate micro-scale parameters of the rock matix of jointed rock mass are determined and listed in Table 1.

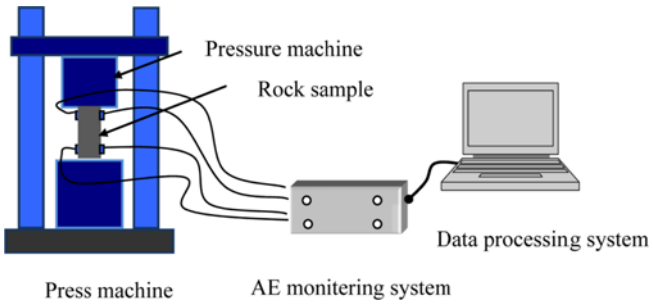

Fig. 2. Schematic diagram of AE monitering system and loading system.

Table 1. Input parameters for contact bonded particle model of Heishan granite

Model	Items	Values
Particle properties	R_{max}/R_{min}	1.66
	Particle density (kg/m^3)	2700.0
	Porosity	14.37%
	Particle contact normal stiffness (N/m)	28.0e9
	Ratio of normal to shear stiffness	1.0
	Friction coefficient	0.8
	Contact bond normal strength Mean value/ Standard deviation (MPa)	100.0/25
Contact bond properties	Contact bond shear strength Mean value/ Standard deviation (MPa)	131.5/30

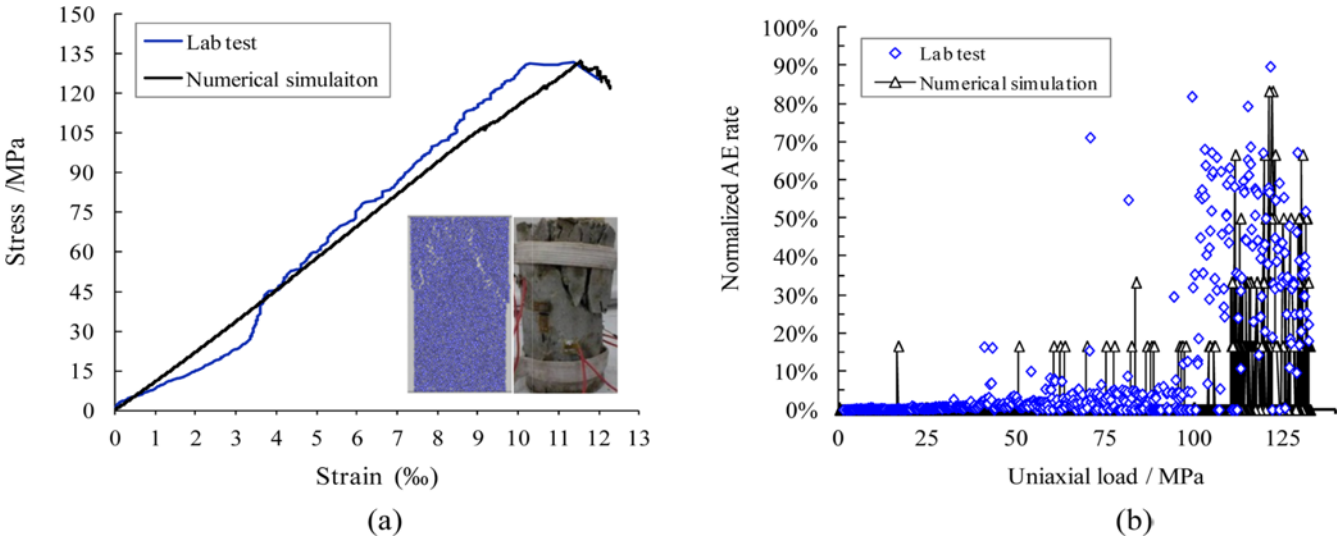

Fig. 3. Comparison of the numerical simulation with the experimental results. (a) Comparison of stress-strain curves and (b) Comparison of AE rates.

3. MECHANICAL BEHAVIOR OF JOINTED ROCK MASSES

A several series of uniaxial compression tests on numerical rock samples containing pre-existing sets of joints have been performed to deal with the effect of joints on the mechanical characteristics of jointed rock mass. The first of these tests concerns the proper strength parameters of the joint model. The joint models an intrinsic property of the two balls in contact. Ivars et al. (2011) discussed a smooth joint contact model shown in Figure 4a. The smooth joint model can specify a given friction angle along a joint plane, without the dilation created by riding over the circular particles. The particle pairs may overlap and slide past each other, instead of being forced to move around one another. The model is bonded with certain normal and shear strength and it allows slip to occur by limiting the shear force after a bond is broken. The spacing between each joint interface is 10 mm and the created interfaces are illustrated as red lines in Figure 4b.

3.1. Strength Parameters for Joint Element

Generally, it is difficult to measure the mechanical properties of the joint or bedding planes directly through laboratory experiments. Bahaaddini et al. (2014) have investigated the effect of joint length on the shear behavior of rough rock joints using PFC2D. They also point out that the nature of scale dependency of rock joints is still unknown and is an ongoing debate. In this section, the procedure to determine the properties of joint is explained. The rock sample with one set of joints whose anisotropy angle is 45° is used comparing with the experimental results by Cho et al. (2012). In the model, different bond strength of joint model is used. K and S is the ratio of bond strength between joint model and intact rock model. The value of K and S are defined by Equations (1) and (2) as follows:

$$K = \frac{n\_bond'}{n\_bond} \times 100\%, \tag{1}$$

$$S = \frac{s\_bond'}{s\_bond} \times 100\%, \tag{2}$$

where n_bond' is the normal bond strength of joint model, n_bond is the normal bond strength of intact rock, s_bond' is the shear bond strength of joint model, s_bond is the shear bond strength of intact rock. There are total twenty scenarios with different K or S. The values are 0 %, 0.1%, 0.5%, 1%, 2%, 3%, 4%, 5%, 6%, 7%, 8%, 9%, 10%, 15%, 30%, 45%, 60%, 75%, 90% and 100%, respectively.

The uniaxial compression stress(UCS), crack initiation stress(CIS) and Young's modulus (E) in the case of layered rock with an angle of 45° are studied under different values of K and S in Figure 5. The crack initiation stress, CIS, rep-

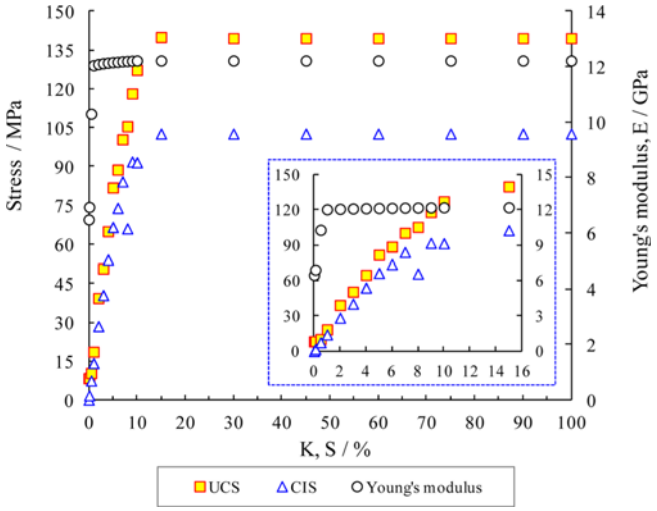

Fig. 5. Variation of UCS, CIS, Young's modulus with increase of K and S value.

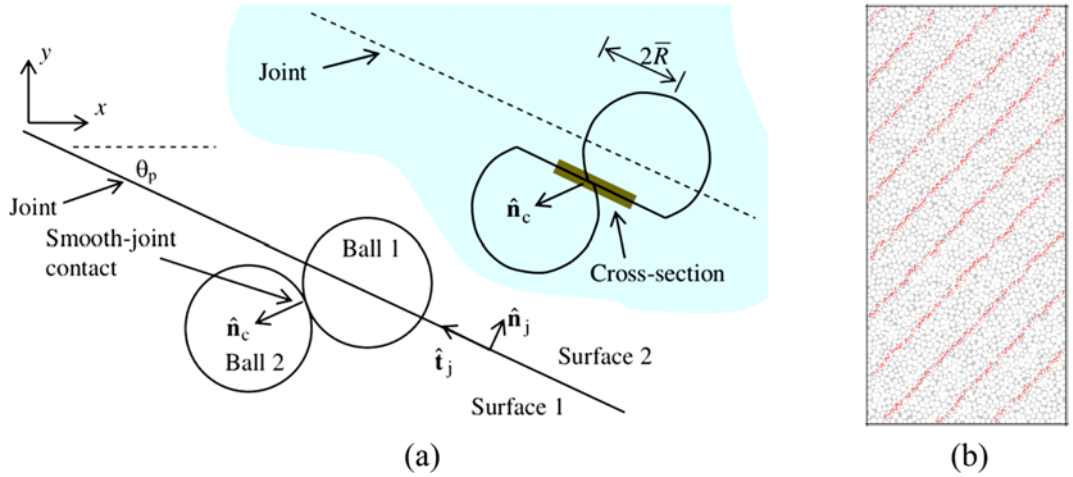

Fig. 4. The effective joint geometry of smooth joint. (a) Effective joint geometry (Ivars et al., 2011) and (b) Stratified rock model in PFC2D.

resents the stress where a certain fraction of total cracks at peak develop in the specimen. In this study, the fraction is 10%. This index will be used to extract the mechanical response upon the jointed rock material. As shown in Figure 5, the influence of joints is apparent when the value of K and S is less than 15%. All the values increase dramatically in the initial stage from 0% to 15% and then tend to be stable with the increase of K and S. The Young's modulus varied from 6.49 GPa to 12.22 GPa, and the ratio of maximum to minimum Young's modulus is 1.88. When the values rise to 15%, the elasticity and peak strength are rarely affected by the layered joints. According to the results, the value should be less than 15% to simulate the real joint elements.

Ten scenarios shown in Figure 6 are carried out with the value of K and S ranging from 0% to 100%. The failure patterns of rock specimen are completely affected by joints when K and S ranges from 0~3% as shown in Figures 6a–c. The fracture planes mainly coincided with the direction of structure plane. When K and S are equal to 5%, two types of failure patterns occur as shown in Figure 6d. The main fracture suface still propagate along the structure plane accompanied with several cracks which are approximately perpendicular to the joint plane. Main fracture that propagated along the structure can still be observed when K and S are equal to 9%. However, the accompanied cracks are more complex than those where K and S is equal to 5%. When K and S increase to 15%, the main fracture surface propagate almost perpendicular to the joint direction instead of along this structure direction, thougth serveral cracks along joint planes near the bottom generate as shown in Figure 6f. In the last several scenarios as shown in Figures 6g and h, the fractures all propagate approximately perpendicular to the structure direction which are similar to the intact rock sample as shown in Figure 6i. The observed result indicates that the failure pattern will not be affected basically by the joint elements. Cho et al. (2012) made some investigations on the failure pattern of schist, shale and gneiss. Based on the experimental results presented in Figure 7, the fracture surfaces in granulite and gneiss propagated mainly along the structure plane. Moreover, there are also two types of cracks according to the failure patterns of schist and shale. Thus, it can be suggested that the influence of joint can be assessed when the value of K and S is in the range of 3~9%. To investigate the mechanical property of jointed rocks quantitatively, the samples with different types of joints will be studied using the value of 5%. The joint parameters including normal stiffness, shear stiffness, friction coefficient, normal bond strength and shear bond strength are listed in Table 2.

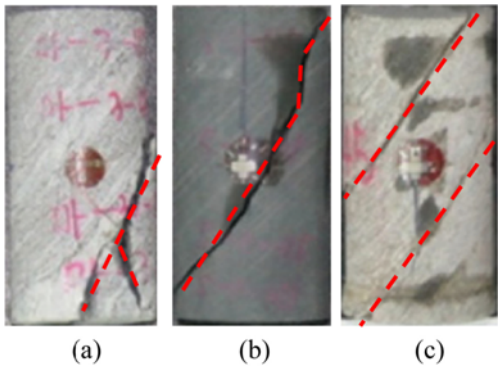

Fig. 7. Failure patterns of specimens under uniaxial compression tests by Cho et al. (2012). (a) Asan gneiss, (b) Boryeong shale and (c) Yeoncheon schist.

Table 2. Input microproperties of joint contact model

Joint model	Value
Joint contact normal stiffness (N/m)	28.0e9
Joint normal to shear stiffness (N/m)	28.0e9
Friction coefficient	0.5
Contact bond normal strength (MPa)	5.0
Contact bond shear strength (MPa)	6.575

3.2. Verifying the Validation of Strength Parameters

To further verify the validity of K (S) value of 5%, a comparison for more joint angles case was carried out for the purpose of validating the accuracy of the joint strength. Seven different numerical models with inclined angles θ of 0°, 15°, 30°, 45°, 60°, 75°, and 90° are analyzed. Figure 8a shows the failure patterns of the specimens in numerical test. The initial crack generally started near the upper boundary in the specimen at θ = 0° and 15°. The rocks mostly failed along

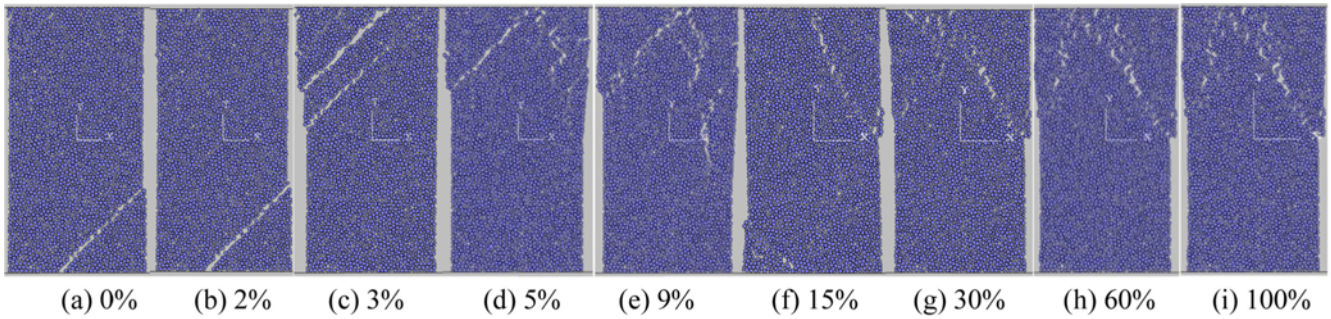

Fig. 6. Numerical results with different K (S) values after failure under uniaxial compression tests.

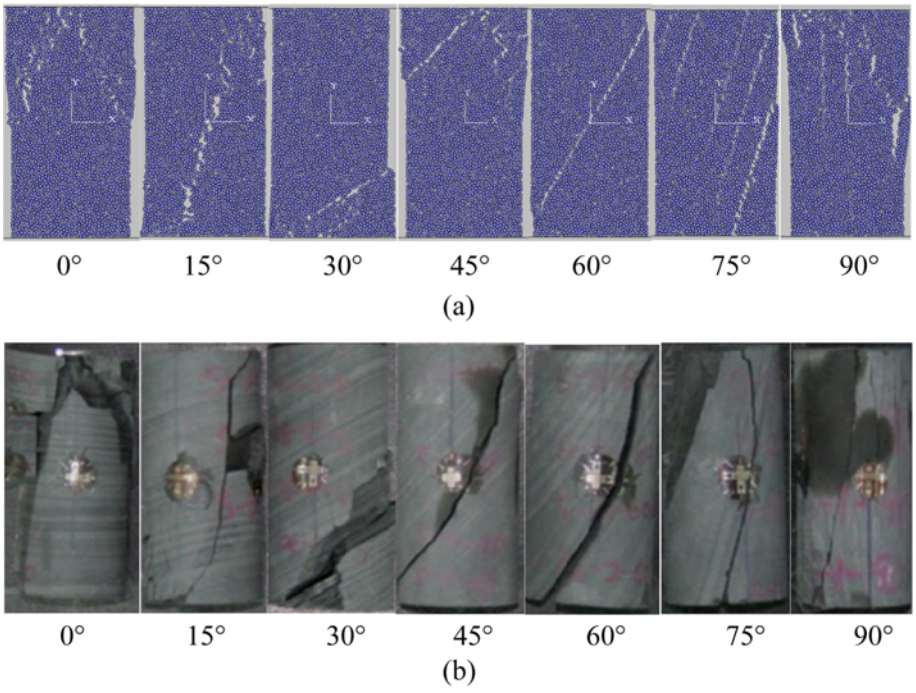

Fig. 8. Comparison of the failure patterns of stratified rocks with different bedding directions with experimental results. (a) Failure patterns in numerical simulation and (b) Lab observations by Cho et al. (2012).

the joint planes when the angle changes from 30° to 90°. The specimen of $\theta = 90°$ fails after the vertical cracks are fully connected. In the presence of fractured specimens, the failure patterns are consistent with the experimental observations (Cho et al., 2012) as shown in Figure 8b. Though the specimen is shale material, a similar failure pattern could, to some extent, verify the reasonability of the microparameters of the PFC2D model.

3.3. Mechanical Properties of Discrete Fracture Network (DFN) Model

The mechanical properties of rock matrix and joint elements are studied in the previous sections. Generally, joints are distributed in jointed rock mass in a complex manner, which make the mechanical properties of rock mass nonlinear, discontinuous and anisotropic. Thus, investigation of

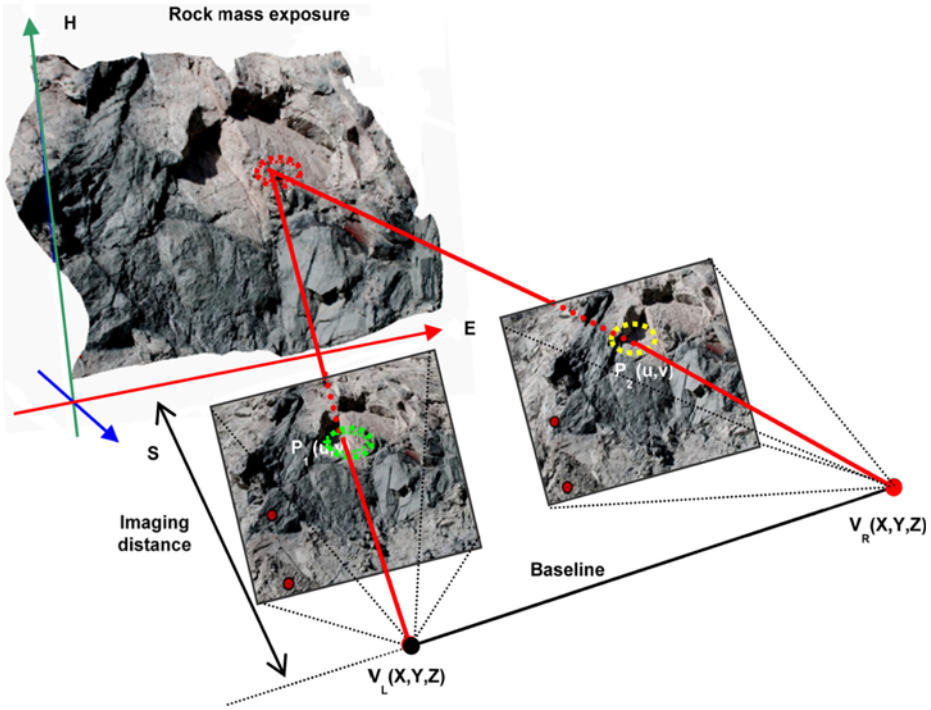

Fig. 9. Imaging principle of the 3D surface measurement.

the mechanical properties of jointed rock mass is of great significance to geoengineering.

In this section, ShapeMetriX3D (3GSM) is used to accurately represent rock discontinuities for the metric acquisition of rock mass exposure and for the measurement of geological parameters by metric 3D images. Stereoscopic photogrammetry deals with the measurement of three-dimensional information from two images showing the same object or surface but taken from two different angles, just as shown in Figure 9. As has been mentioned by Wang et al. (2013), a pair of corresponding image points $P_1(u,v)$ and $P_2(u,v)$ imaging rays (colored in red) are reconstructed whose intersection leads to a 3D surface point P (X,Y,Z) from the determined orientation between the two images. By automatic identification of corresponding points within the image pair, the result of the acquisition is a metric 3D image that covers the geometry of the rock exposure. Once the image of a rock wall is ready, geometric measurements can be taken.

According to the survey results as shown in Figure 10a, the geologic data like joint density, dip angle, trace length and spacing is listed in Table 3. Four different probability statistical models are used to generate the discrete fracture network model. The dip angle, dip direction, trace length and spacing are all follow one particular probability statistical model. Type I of the probability statistical model for negative exponential distribution, Type II for normal distribution; Type III for logarithmic normal distribution and Type IV for uniform distribution. The DFN model is then generated using the Monte Carlo method and is imported into PFC2D using FISH development language (Wang et al., 2013) as shown in Figure 10b. On this basis, a serial of uniaxial compressive tests could be brought out to study the size effect, representive elementary volume (REV) and anisotropic properties of jointed rock mass.

3.3.1. Size effect and anisotropy of elastic properties

The REV of jointed rock masses is one whose scale is

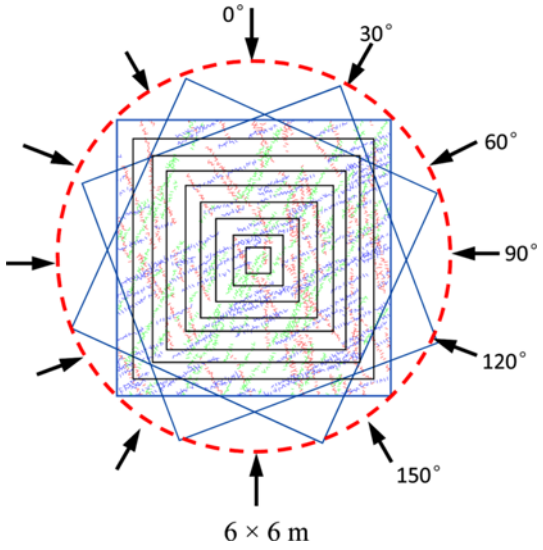

Fig. 11. Schematic diagram of studying scale effect and anisotropy.

Table 3. Characteristics of three sets of discontinuities for the slope exposure

Set	Density (m^{-1})	Dip angle (°)			Trace length (m)			Fault throw (m)			Spacing (m)		
		Type	Avg.	Dev.	Type	Avg.	Dev.	Type	Avg.	Dev.	Type	Avg.	Dev.
1	1.2	III	71.24	15.05	II	0.86	0.23	IV	0.23	0.04	IV	0.83	0.75
2	1.3	IV	59.85	8.40	II	0.89	0.28	II	0.29	0.17	IV	0.76	0.73
3	3.3	III	55.29	13.35	II	0.85	0.25	II	0.26	0.16	IV	0.30	0.31

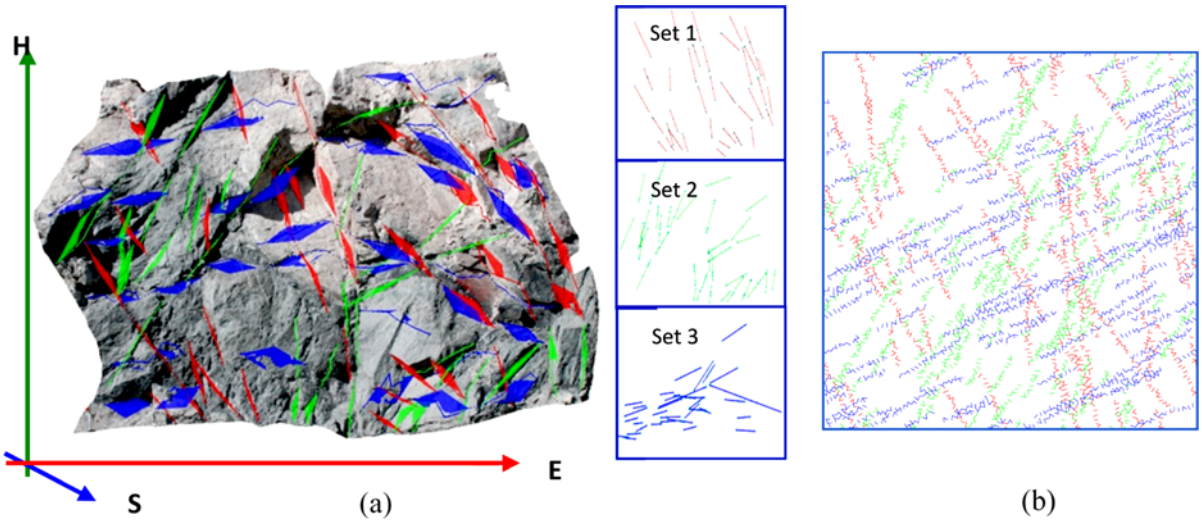

Fig. 10. Geological mapping of stereoscopic restructuring model and the generated fracture network by Monte Carlo method in PFC2D with size of 6 × 6 m. (a) Geological mapping and (b) Discrete fracture network in PFC2D.

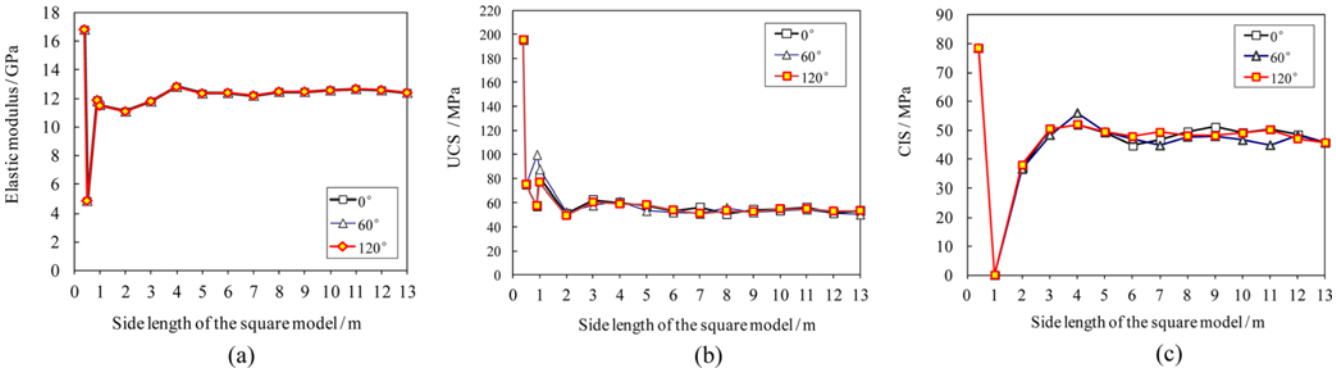

Fig. 12. Variation of the mechanical properties with the increase of scale size when $\theta = 0°$, $\theta = 60°$ and $\theta = 120°$. (a) Elastic modulus, (b) Uniaxial compressive strength (UCS) and (c) Crack initiation stress (CIS).

large enougth that the certain property does not significantly change. Thus, it could be regarded as a quantitative criterion for choosing appropriate parameters for equivalent continuum methods. In this section, the scale effects, REV and anisotropic properties will be studied by PFC2D method by considering different sizes and anisotroy angles. Figure 11 shows the schematic diagram of studying scale effect and anisotropy. Rotated every 30° clockwise, the elastic modulus, uniaxial compressive strength, and crack initiation stress of different directions could be acquired. By enlarging the geometric size of the fracture network, the elasticity and strength scale effect can be investigated finally. Discrete fracture network models of different sizes $l = 0.4 \times 0.4$ m, 0.5×0.5 m, 0.9×0.9 m, 1×1 m, 2×2 m, 3×3 m, 4×4 m, 5×5 m, 6×6 m, 7×7 m, 8×8 m, 9×9 m, 10×10 m, 11×11 m, 12×12 m and 13×13 m, have been generated and tested using numerical uniaxial compressive tests.

For each discrete fracture network, the elastic modulus is obtained. Figure 12a shows the elastic modulus of the samples with varied scale sizes and joint orientations. Now, we take, for example, the rock sample with anisotropic angle at $\theta = 120°$ to estimate the REV size of the jointed rock mass.

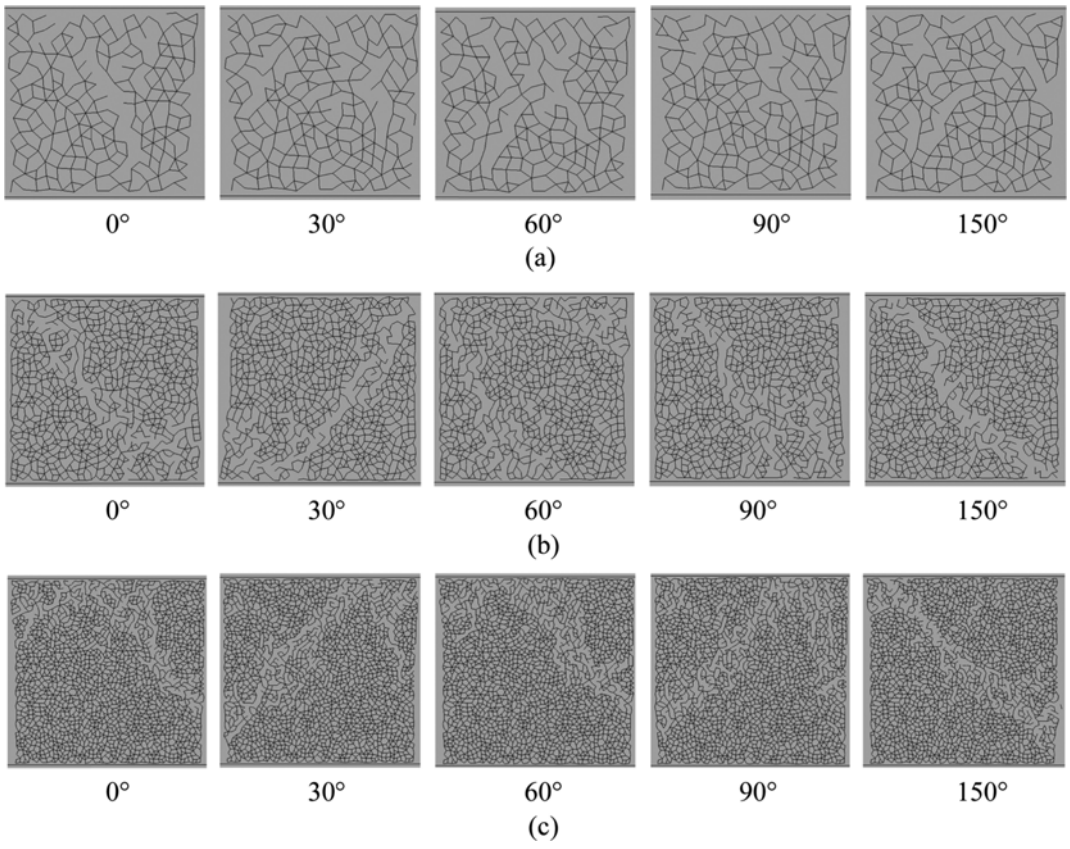

Fig. 13. Variation of failure patterns with different sacle sizes. (a) 2×2 m, (b) 4×4 m and (c) 6×6 m.

The values of elastic modulus decrease with the scale size increasement. When the model size increases up to 6m, the elastic modulus comes to 12.38 GPa and tends to stabilize. Figure 12b presents the relationship between the uniaxial compressive strength (UCS) and the sizes of the rock mass. A decrease of the UCS, which converges to a limit value, can be observed when the sample size increases. The values tend to be 53.86 MPa at $\theta = 120°$ after the model size increases up to 6 m. A similar trend is also observed by analysing the scale effect of crack initiation stress (CIS) in Figure 12c. Thus, the REV size of the jointed rock sample can be preliminarily chosen as 6 × 6 m according to the trends of the variations.

3.3.2. Failure patterns

The representative elementary volume (REV) size of the jointed rock mass is estimated to be 6 × 6 m after the comprehensive numerical analysis on the elastic modulus, uniaxial compressive strength and the crack initiation stress of the jointed rocks at different spatial scales and joint orientations. According to the concept of REV, the mechanical properties should stabilize with the increase of its sizes. Figure 13 shows the failure patterns of jointed rock mass at different scale sizes. In each scenario, five anisotropic angles of joints at θ = 0°, 30°, 60°, 90° and 150° are studied. In the models, the black items represent the contact bonds between particles. According to Figure 13a, the failure patterns completely differ from each other when scale size is 2 × 2 m. In addition, the anisotropy of failure pattern is relatively apparent. Figure 13b presents the failure patterns of samples with size of 4 × 4 m and they are still different. In particular, the failure patterns of the specimens do not tend to stabilize when the size comes to the REV size (6 × 6 m) as shown in Figure 13c. There still exist four different failure patterns. Thus, it is indicated that the REV size of the jointed rock mass should not be 6 × 6 m.

To study the proper REV size, three more scenarios with scale size of 7 × 7 m, 8 × 8 m and 9 × 9 m, are brought out and presented in Figure 14. As shown in Figures 14a and b, different failure modes still exist with the variation of anisotropic angles. When the size comes to 9 × 9 m, the failures patterns are basically similar as shown in Figure 14c. The REV size is revised to be 9 × 9 m according to the scale effect study of failure patterns.

To further validate the REV size, the specimens with the size of 11 × 11 m and 12 × 12 m are studied in Figures 15a and b, respectively. In the scenario of 11 × 11 m, the failure patterns in five different joint orientations are apparently similar.

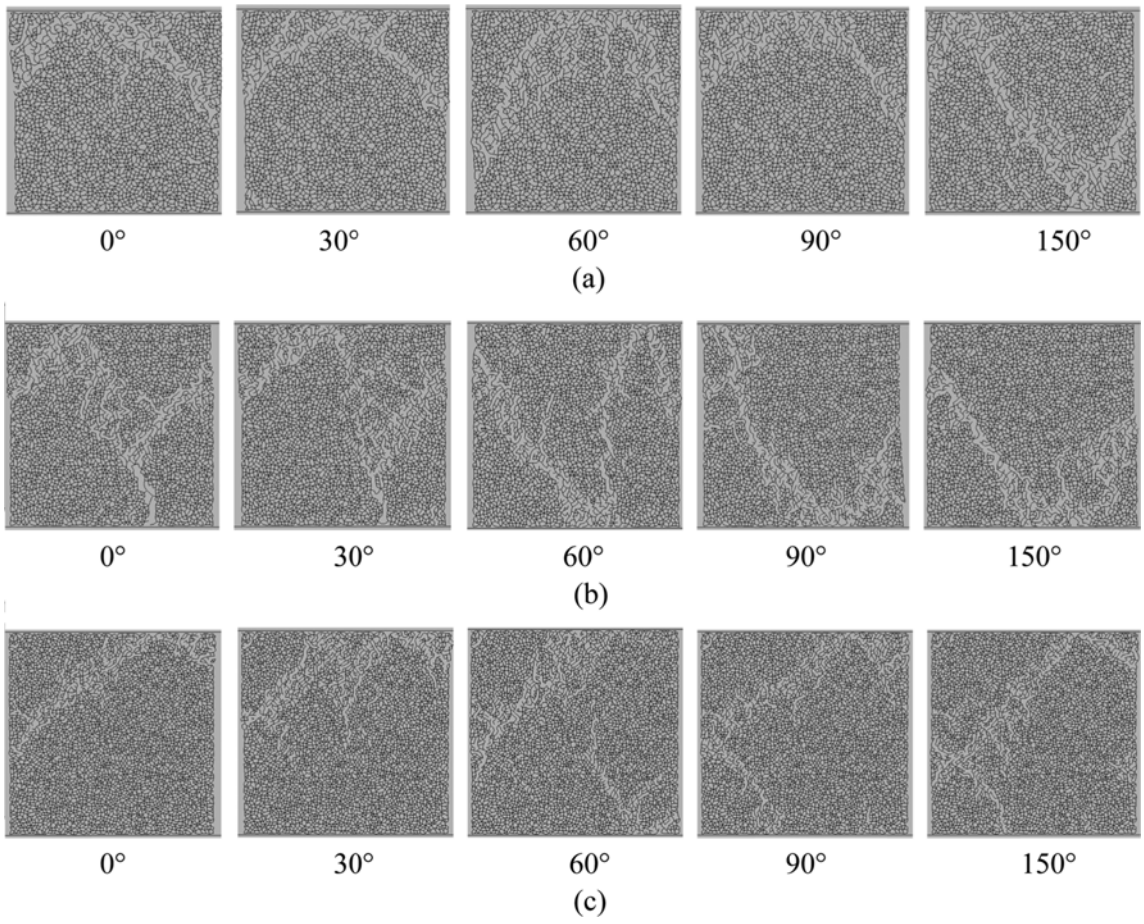

Fig. 14. Variation of failure patterns with different sacle sizes. (a) 7 × 7 m, (b) 8 × 8 m and (c) 9 × 9 m.

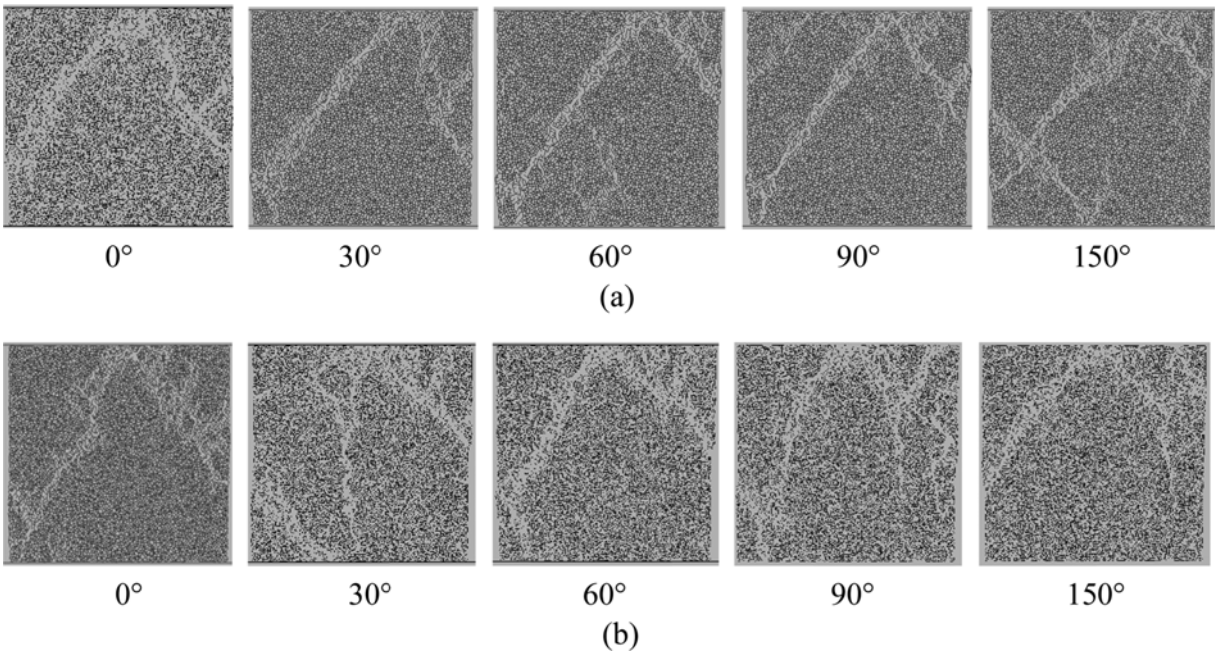

Fig. 15. Variation of failure patterns with different scale sizes. (a) 11 × 11 m and (b) 12 × 12 m.

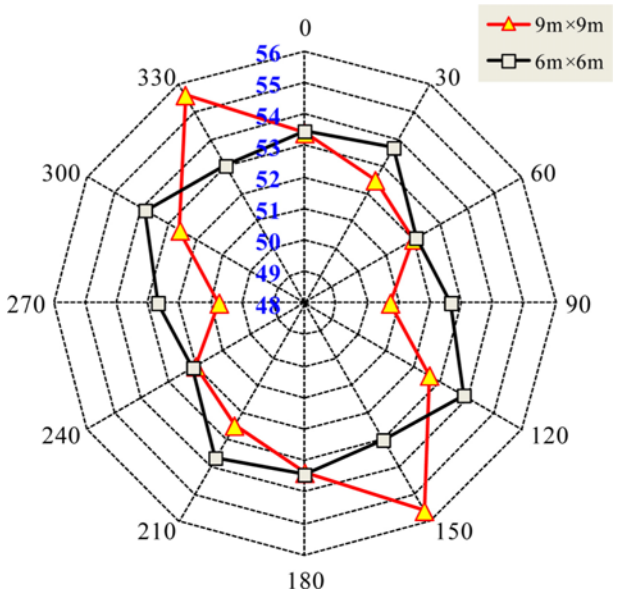

Fig. 16. Comparison of directional uniaxial compressive strength contour for DFN model of 9 × 9 m with that of 6 × 6 m (Unit: MPa).

Moreover, the similar failure patterns are also observed in the situation of 12 × 12 m. According to the results, the scale size of 9 × 9 m can be treated as a representative elementary volume size. Beyond this size, no distinct scale effect of failure pattern is noticed. Besides, the anisotropy of failure patterns is not apparent any more for the highly jointed rocks.

Figure 16 presents the directional uniaxial compressive strength (UCS) for jointed rock model at the sizes of 6 × 6 m and 9 × 9 m. Needless to say, the UCS is affected significantly by the existence of the joints. In the scenario of 6 × 6 m, the principal values of UCS is 52.1 MPa for minimum and 53.86 MPa for maximum. The principal direction angle is approximately 120° and the ratio of maximum to minimum value is about 1.03. For REV size of 9 × 9 m, the values of uniaxial compressive strength vary with the variation of anisotropy angles and the principal direction angle is approximately 150°. The maximum value of UCS is 55.62 MPa and minimum is 50.73 MPa. The anisotropic ratio of UCS is 1.10 which is higher than the scenario of 6 × 6 m. According to the result, an engineering errors may exsit when the REV size is studied without considering the failure pattern. The findings will help to determine the scale parameters in Heishan metal mine and investigate the geomechanical properties of jointed rock mass.

4. CONCLUSIONS

This paper reports the numerical investigation of deformation and strength behavior of jointed rock mass. The microparameters for granite was calibrated based on uniaxial compression and acoustic emission tests. Both the complete stress-strain relation and acoustic emission rate in DEM simulaiton were in good agreement with the experimental test. The ratio of joint bond strength to intact rock bond strength was in the range from 3% to 9% both in shear and normal directions according to the comparison of failure pattern in numerical results with the existing experimental results. In the jointed rock samples with varied joint angles, similar failure patterns were also observed when the ratio value of 5% was used. The intact rock combined with in situ disconti-

nuities was modeled and the scale effect on elasticity and strength were studied. The failure pattern of the jointed rock mass was introduced to study the scale effect and the revised REV size was 9 × 9 m according to the failure pattern analysis. It is suggested that the failure pattern should be considered in the REV and anisotropy study for jointed rock mass. The results will help to determine the scale parameters in Heishan metal mine and investigate the geomechanical properties of jointed rock mass.

ACKNOWLEDGMENTS: The work was financially supported by the National Science & Technology Support Project (No. 2013BAB02B08) and the Fundamental Research Funds for the Central Universities (No. FRF-TP-15-109A1). The Natural Science Foundation of China (No. 51174045, 41172265, 11572344) also gives financial support to this research. All these supports are gratefully acknowledged.

REFERENCES

Bahaaddini, M., Hagan, P.C., Mitra, R., and Hebblewhite, B.K., 2014, Scale effect on the shear behaviour of rock joints based on a numerical study. Engineering Geology, 181, 212–223.

Cho, J.W., Kim, H., Jeon, S., and Min, K.B., 2012, Deformation and strength anisotropy of Asan gneiss, Boryeong shale, and Yeoncheon schist. International Journal of Rock Mechanics and Mining Sciences, 50, 158–169.

Cho, N., Martin, C.D., and Sego, D.C., 2007, A clumped particle model for rock. International Journal of Rock Mechanics and Mining Sciences, 44, 997–1010.

Cundall, P.A. and Strack, O.D., 1979, A discrete numerical model for granular assemblies. Geotechnique, 29, 47–65.

Dershowitz, W.S. and Einstein, H.H., 1988, Characterizing rock joint geometry with joint system models. Rock Mechanics and Rock Engineering, 21, 21–51.

Fakhimi, A. and Gharahbagh, E.A., 2011, Discrete element analysis of the effect of pore size and pore distribution on the mechanical behavior of rock. International Journal of Rock Mechanics and Mining Sciences, 48, 77–85.

Funatsu, T. and Shimizu, N., 2011, Numerical simulation of crack propagation in rock by clumped particle model. In: Qian, Q.H. and Zhou, Y.X. (eds.), Proceedings of the 12th ISRM International Congress on Rock Mechanics: Harmonising rock engineering and the environment, Beijing, Oct. 18–21, p. 387–390.

Hazzard, J.F. and Young, R.P., 2000, Simulation acoustic emissions in bonded-particle models of rock. International Journal of Rock Mechanics and Mining Sciences, 37, 867–872.

Holt, R.M., Kjølaas, J., Larsen, I., Li, L., Pillitteri, A.G., and Sønstebø, E.F., 2005, Comparison between controlled laboratory experiments and discrete particle simulations of the mechanical behaviour of rock. International Journal of Rock Mechanics and Mining Sciences, 42, 985–995.

Itasca Consulting Group, Inc., 2004, Particle Flow Code in 2-Dimensions, Command Reference version 3.1. Minneapolis.

Itasca Consulting Group, Inc., 2004, Particle Flow Code in 2-Dimensions, Theory and Background v3.1. Minneapolis.

Ivars, D.M., Pierce, M.E., Darcel, C., Montes, J.R., Potyondy, D.O., Young, R.P., and Cundall, P.A., 2011, The synthetic rock mass approach for jointed rock mass modeling. International Journal of Rock Mechanics and Mining Sciences, 48, 219–244.

Lee, S.E. and Jeong, G.C., 2015, Numerical analysis on micro-damage in bisphere model of granitic rock. Geosciences Journal, 19, 135–144.

Pariseau, W.G., Puri, S., and Schmelter, S.C., 2008, A new model for effects of impersistent joint sets on rock slope stability. International Journal of Rock Mechanics and Mining Sciences, 45, 122–131.

Park, B. and Min, K., 2012, Discrete element modelling of shale as a transversely isotropic rock. 7th Asian Rock Mehcanics Symposium on the Present and Future of Rock Engineering, Seoul, Oct. 15–19, p. 336–342.

Potyondy, D.O. and Cundall, P.A., 2004, A bonded-particle model for rock. International Journal of Rock Mechanics and Mining Sciences, 41, 1329–1364.

Sarfarazi, V., Ghazvinian, A., Schubert, W., Blumel, M., and Nejati, H.R., 2014, Numerical simulation of the process of fracture of echelon rock joints. Rock Mechanics and Rock Engineering, 47, 1355–1371.

Wang, C., Tannant, D.D., and Lilly, P.A., 2003, Numerical analysis of the stability of heavily jointed rock slopes using PFC2D. International Journal of Rock Mechanics and Mining Sciences, 40, 415–424.

Wang, P.T., Yang, T.H., Yu, Q.L., Liu, H.L., and Zhang, P.H., 2013, Characterization on jointed rock masses based on PFC2D. Frontiers of Structural and Civil Engineering, 7, 32–38.

Wang, P.T., Yang, T.H., Xu, T., Yu, Q.L., and Liu, H.L., 2013, A Model of Anisotropic Property of Seepage and Stress for Jointed Rock Mass. Journal of Applied Mathematics, 2013, Article ID 420536, 19 p.

Wasantha, P.L.P., Ranjith, P.G., Xu, T., Zhao, J., and Yan, Y.L., 2014, A new parameter to describe the persistency of non-persistent joints. Engineering Geology, 181, 71–77.

Xu, T., Ranjith, P.G., Wasantha, P.L.P., Zhao, J., Tang, C.A., and Zhu, W.C., 2013, Influence of the geometry of partially-spanning joints on mechanical properties of rock in uniaxial compression. Engineering Geology, 167, 134–147.

Yoon, J., 2007, Application of experimental design and optimization to PFC model calibration in uniaxial compression simulation. International Journal of Rock Mechanics and Mining Sciences, 44, 871–889.

Zhang, X.P. and Wong, L.N.Y., 2013, Crack initiation, propagation and coalescence in rock-like material containing two flaws, a numerical study based on bonded-particle model approach. Rock Mechanics and Rock Engineering, 46, 1001–1021.

Zhao, Y.L., Wan, W., Wang, W.J., Wang, M., and Peng, Q.Y., 2013, Fracture experiments on ordered multi-crack body in rock-like materials under uniaxial compression and numerical simulation of wing cracks. Chinese Journal of Geotechnics and Engineering, 35, 2097–2109. (in Chinese)

Manuscript received September 9, 2015
Manuscript accepted December 3, 2015